PROCEEDINGS OF THE ROYAL SOCIETY A MATHEMATICAL, PHYSICAL & ENGINEERING SCIENCES

Nonlinear low-frequency gravity waves in a water-filled cylindrical vessel subjected to high-frequency excitations

Chunyan Zhou, Dajun Wang, Song Shen and Jing Tang Xing

Proc. R. Soc. A 2013 **469**, 20120536, published 6 March 2013

PROCEEDINGS OF THE ROYAL SOCIETY A

rspa.royalsocietypublishing.org

Research

Cite this article: Zhou C, Wang D, Shen S, Xing JT. 2013 Nonlinear low-frequency gravity waves in a water-filled cylindrical vessel subjected to high-frequency excitations. Proc R Soc A 469: 20120536.
http://dx.doi.org/10.1098/rspa.2012.0536

Received: 10 September 2012
Accepted: 5 February 2013

Subject Areas:
mechanics, wave motion

Keywords:
nonlinear fluid–structure interactions, dragon washbasin, nonlinear-free surface wave, transition of gravity waves, nonlinear vibration

Author for correspondence:
Dajun Wang
e-mail: wdjwdy@pku.edu.cn

Nonlinear low-frequency gravity waves in a water-filled cylindrical vessel subjected to high-frequency excitations

Chunyan Zhou[1], Dajun Wang[2], Song Shen[3] and Jing Tang Xing[4]

[1]Key Laboratory of Dynamics and Control of Flight Vehicle, Ministry of Education, School of Aerospace Engineering, Beijing Institute of Technology, Beijing 100081, People's Republic of China
[2]Department of Mechanics and Engineering Science and LTCS, College of Engineering, Peking University, Beijing 100081, People's Republic of China
[3]Orient Institute of Vibration and Noise, Beijing 100085, People's Republic of China
[4]Fluid–Structure Interaction Research Group, Faculty of Engineering and the Environment, University of Southampton, Southampton SO17 1BJ, UK

In the experiments of a water storage cylindrical shell, excited by a horizontal external force of sufficient large amplitude and high frequency, it has been observed that gravity water waves of low frequencies may be generated. This paper intends to investigate this phenomenon in order to reveal its mechanism. Considering nonlinear fluid–structure interactions, we derive the governing equations and the numerical equations describing the dynamics of the system, using a variational principle. Following the developed generalized equations, a four-mode approximation model is proposed with which an experimental case example is studied. Numerical calculation and spectrum analysis demonstrate that an external excitation with sufficient large amplitude and high frequency can produce gravity water waves with lower frequencies. The excitation magnitude and frequencies required for onset of the gravity waves are found based on the model. Transitions between different gravity waves are also revealed through the numerical analysis. The findings developed by this method are validated by available experimental observations.

1. Introduction

In 1954, the famous paper by Benjamin & Ursell [1] investigated the half-frequency subharmonic resonance induced on the liquid surface by a vertical vibration of the container, and this work has been greatly extended by Couder *et al.* [2] to show a wave–particle duality. The mechanism of this type of subharmonic resonance in nonlinear dynamical systems has been well investigated and modelled (for example, the book by Guckenheimer & Holmes [3]). Therefore, we do not intend to discuss this type of phenomena in this short paper but we try to address the mechanism of the phenomenon described by Huntley [4], who discovered another type of large amplitude gravity waves of lower frequencies, produced in a half water-filled cylindrical beaker subjected to a more high-frequency horizontal excitation. When a water-filled beaker is subjected to an excitation of frequency near to one of natural bell modes of the structure, large amplitude standing water waves may be generated. The frequency of standing wave is about one-fiftieth of the excitation frequency, which is not like the half-frequency subharmonic resonance mentioned at the beginning of this introduction. It was reported that if the bell mode, in the form of $\cos m\theta$ or $\sin m\theta$ around the circumference of the beaker, had a wavenumber $m \geq 2$, then the aroused standing waves might have a wavenumber of either 0 (axisymmetrical modes) or $2m$. Because no special relationship exists between the high-excitation frequency and frequencies of the standing waves, this phenomenon was not explained as Faraday waves by parametric resonant theory. Mahony & Smith [5] proposed an idealized model to explain this as a 'spatial resonant' phenomenon by considering the interactions between acoustic air and water waves in a rectangular organ pipe partially filled with water when the air being excited in a resonant organ pipe mode. Their investigation developed an equation governing the critical amplitude of solid boundary vibration with respect to excitation frequency, which was validated by the experimental results. Huntley [6] extended Mahony & Smith's model to real three-dimensional cases. As reported by Wei *et al.* [7], Wang observed and systematically studied the same phenomenon while doing some experimental research on the dragon washbasin. Being interested in Wang's experiments, Wei *et al.* [7], Hsieh & Denissenko [8], Li [9] and Shen [10] further experimentally and/or theoretically investigated nonlinear water waves produced by a prescribed vessel motion. Hsieh [11] presented a parametric resonance model and numerically demonstrated the existence of low-frequency gravity waves.

However, the reported theoretical researches concentrated only on the water waves in the fluid domain excited by prescribed vessel motions. Physically, what is involved here is a typical fluid–structure interaction (FSI) problem, so that a consideration of FSI is necessary. This paper intends to address this gap to consider nonlinear water–shell interactions to reveal the possible mechanism. In the first instance, to avoid the numerical difficulty of the shell nonlinearity, we assume a small deformation of the shell governed by a linearized theory. The water is considered as an incompressible fluid with large nonlinear waves on the free surface. A variational principle of nonlinear FSI system is used to derive the approximate solutions of this nonlinear system.

2. The problem and variational formulation

As shown in figure 1, a water–shell-coupled system consists of a thin linear elastic cylindrical shell of thickness Δh, height b, radius a, elastic modulus E, Poisson's ratio ν and mass density ρ_S and the partially filled water of depth d and mass density ρ_F. The lower bottom of the shell is fixed and its upper end is free. Let r, θ and z be a cylindrical coordinate system of which its origin O is at the intersection point of the shell centre line and the static equilibrium water surface. The water is assumed to be invicid, incompressible and irrotational, then its motion can be described by a potential function $\phi(r, \theta, z)$. A horizontal sinusoidal excitation force $F \sin \Omega t$ of amplitude F and frequency Ω is applied at a point on the outside surface of shell in the height of water. The S_F and S_F^0 denote the current and static-free surfaces of the fluid, respectively, whereas S_W and S_W^0 are the current and static wet surfaces between the shell and the water, respectively.

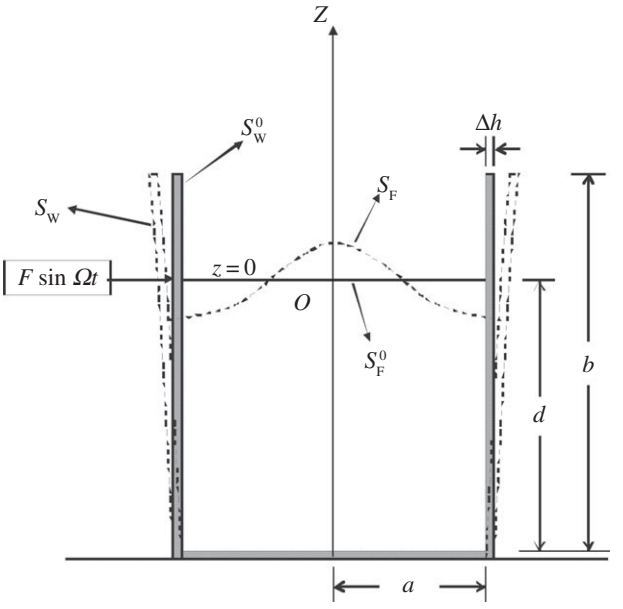

Figure 1. Elastic shell–water interaction system.

The displacement components in directions of z, θ, r of the shell middle surface are denoted by u, v, w, respectively. A large wave height $\eta(r, \theta, t)$ on the water surface is assumed, so that the nonlinearity of the system must to be considered. The current-free surface (S_F) and wet surface (S_W) can be respectively represented by the following equations

$$S_F(z, r, \theta, t) = z - \eta(r, \theta, t) = 0 \tag{2.1}$$

and

$$S_W(r, \theta, z, t) = r - a - w(z, \theta, t) = 0. \tag{2.2}$$

The variational principle for fluid dynamics in Eulerian description was developed by Luke [12] and Seliger & Whitham [13]. The variational principle for generalized nonlinear FSI dynamics was presented by Xing & Price [14], from which the dynamics of a shell–water interaction system is governed by the variation

$$\delta J(\phi, \eta, u, v, w) = \delta \int_{t_1}^{t_2} L \mathrm{d}t \equiv \delta \int_{t_1}^{t_2} (L_F + L_S)\, \mathrm{d}t = \delta W. \tag{2.3}$$

The vanishing of this variation leads to the governing equations and boundary conditions of the problem. In this expression,

$$L_F = -\int\int\int \rho_F \left(\phi_t + \frac{1}{2}\nabla\phi \cdot \nabla\phi + gz\right) \mathrm{d}v \tag{2.4}$$

and

$$L_S = T_S(\dot{u}, \dot{v}, \dot{w}) - V_S(u, v, w), \tag{2.5}$$

where $V_S(u, v, w)$ and $T_S(\dot{u}, \dot{v}, \dot{w})$, as given in appendix A, represent the potential energy and kinetic energy of the shell, respectively. The δW denotes the virtual work of the excitation force

$$\delta W = \int_{t_1}^{t_2} \delta w\,(0, 0, t)\, F \sin \Omega t\, \mathrm{d}t. \tag{2.6}$$

It should be mentioned that the variables describing the fluid motion are defined in the Euler space, but the variables describing the shell motion are defined in the material space. The fluid

domain is a movable domain and its boundary (the S_F together with the S_W) is movable owing to the motion. On noting these differences involving the variation of the functional, as described by Xing & Price [14], the stationary conditions of the variation of functional (2.3) provide the dynamic equations describing the nonlinear FSI system.

3. Discrete nonlinear equations

(a) Rayleigh–Ritz expansions

Based on the Rayleigh–Ritz approach [15], the velocity potential $\phi(r,\theta,z,t)$ and free surface height $\eta(r,\theta,t)$ of the fluid as well as the shell displacement $\mathbf{w}(\theta,z,t)=[uvw]^{\mathrm{T}}$ can be represented by the summations of the corresponding Ritz functions, respectively. The fluid Ritz functions $\phi(r,\theta,z,t)$ should satisfy the boundary condition $\partial\phi/\partial z=0$ on the water base $z=-d$. The shell functions are the dry shell's natural modes satisfying its base displacement condition. Other boundary conditions as well as governing equations describing FSIs, such as nonlinear conditions on the free surface and the shell–water interaction, will be satisfied by the stationary conditions of the variational principle demonstrated by Xing & Price [14]. According to Hsieh [11], the influence of contact line conditions at the edge of the water surface on the shape of wave motion could be neglected, thus the velocity potential $\phi(r,\theta,z,t)$ and the wave height $\eta(r,\theta,t)$ are represented by

$$\phi(r,\theta,z,t)=\phi_{00}(t)\ln r+\sum_{n=1}^{\infty}\phi_{0n}(t)r^n\cos n\theta+\sum_{n=1}^{\infty}\sum_{m=1}^{\infty}\phi_{mn}(t)I_n\left(\frac{m\pi r}{d}\right)\cos n\theta\cos\frac{m\pi z}{d}$$
$$+\sum_{n=1}^{\infty}\sum_{l=1}^{\infty}\phi_{ln}(t)J_n(\lambda_{l,n}r)\cos n\theta\cosh\lambda_{ln}(z+d) \tag{3.1}$$

and

$$\eta(r,\theta,t)=\sum_{n=1}^{\infty}\sum_{l=1}^{\infty}\eta_{ln}(t)J_n(\lambda_{l,n}r)\cos n\theta, \tag{3.2}$$

respectively, where $J_n(\,)$ and $I_n(\,)$ are Bessel functions and λ_{ln} is the solution of equation

$$J_n'(\lambda_{l,n}a)=0,\quad l=1,2,\ldots, \tag{3.3}$$

and $\phi_{ln}(t)$ and $\eta_{ln}(t)$ represent the generalized coordinates corresponding to their Ritz functions, respectively. By choosing L and M terms for equations (3.1) and (3.2), respectively, we obtain the following matrix forms

$$\varphi(r,\theta,z,t)=\boldsymbol{\Phi}(r,\theta,z)\boldsymbol{\varphi}(t),\quad \boldsymbol{\Phi}=\begin{bmatrix}\Phi_1 & \Phi_2 & \cdots & \Phi_L\end{bmatrix}\quad\text{and}\quad \boldsymbol{\varphi}=\begin{bmatrix}\varphi_1 & \varphi_2 & \cdots & \varphi_L\end{bmatrix}^{\mathrm{T}} \tag{3.4}$$

and

$$\eta(r,\theta,t)=\mathbf{H}(r,\theta)\boldsymbol{\eta}(t),\quad \mathbf{H}=\begin{bmatrix}H_1 & H_2 & \cdots & H_M\end{bmatrix}\quad\text{and}\quad \boldsymbol{\eta}=\begin{bmatrix}\eta_1 & \eta_2 & \cdots & \eta_M\end{bmatrix}^{\mathrm{T}}. \tag{3.5}$$

The displacement of shell is represented, using the natural modes of dry shell

$$w(\theta,z,t)=\mathbf{W}(\theta,z)\mathbf{w}(t),\quad \mathbf{W}=\begin{bmatrix}W_1 & W_2 & \cdots & W_N\end{bmatrix}\quad\text{and}\quad \mathbf{w}=\begin{bmatrix}w_1 & w_2 & \cdots & w_N\end{bmatrix}^{\mathrm{T}}. \tag{3.6}$$

Here, the Ritz functions Φ_i, $(i=1,2,\ldots,16)$, H_j, $(j=1,2,\ldots,8)$ and W_i, $(i=1,2,\ldots,4)$ are listed in appendix A.

(b) Fluid Lagrangian function

A substitution of equations (3.4) and (3.5) into (2.4) gives

$$L_{\mathrm{F}} = -\boldsymbol{\varphi}^{\mathrm{T}}\mathbf{b} - \frac{\boldsymbol{\varphi}^{\mathbf{T}}\mathbf{C}\boldsymbol{\varphi}}{2} - V_{\mathrm{F}}. \tag{3.7}$$

Here, $\mathbf{C}$ is a symmetric matrix with its elements

$$C_{lm} = \rho_{\mathrm{F}} \int\int\int (\nabla\Phi_l \cdot \nabla\Phi_m)\, \mathrm{d}v = \rho_{\mathrm{F}} \int_{z=-d}^{\eta} \int_{r=0}^{a+w} \int_{\theta=0}^{2\pi} (\nabla\Phi_l \cdot \nabla\Phi_m) r\, \mathrm{d}\theta\, \mathrm{d}r\, \mathrm{d}z, \quad l,m = 1,2,\ldots,L, \tag{3.8}$$

$\mathbf{b}$ is a column vector with its elements

$$b_l = \rho_{\mathrm{F}} \int\int\int \Phi_l\, \mathrm{d}v = \rho_{\mathrm{F}} \int_{z=-d}^{\eta} \int_{r=0}^{a+w} \int_{\theta=0}^{2\pi} \Phi_l r\, \mathrm{d}\theta\, \mathrm{d}r\, \mathrm{d}z, \quad l = 1,2,\ldots,L, \tag{3.9}$$

and V_{F} is a scalar quantity representing the gravity potential of water

$$V_{\mathrm{F}} = \int\int\int \rho_{\mathrm{F}} g z\, \mathrm{d}v = \rho_{\mathrm{F}} g \int_{z=-d}^{\eta} \int_{r=0}^{a+w} \int_{\theta=0}^{2\pi} z r\, \mathrm{d}\theta\, \mathrm{d}r\, \mathrm{d}z. \tag{3.10}$$

In these formulations, the wet boundary and free surface of the fluid domain are related to the shell and water motions, $0 \le r \le a + w(\theta, z, t)$ and $-d \le z \le \eta(r, \theta, t)$, so that the integrals in (3.8)–(3.10) are dependent of $\eta(r, \theta, t)$ and $w(\theta, z, t)$. Introducing a generalized vector

$$\mathbf{q} = \begin{bmatrix} \boldsymbol{\eta}^{\mathrm{T}} & \mathbf{w}^{\mathrm{T}} \end{bmatrix}^{\mathrm{T}}, \tag{3.11}$$

we derive the matrices $\mathbf{C}$, $\mathbf{b}$ and the function V_{F} as nonlinear functions of $\mathbf{q}$ in appendix B.

(c) Shell Lagrangian function

Substituting equation (3.11) into (2.5) and using the orthogonal relationships of shell natural modes, we obtain the Lagrangian function of the shell in the matrix form

$$L_{\mathrm{S}} = T_{\mathrm{S}} - V_{\mathrm{S}} = \frac{\dot{\mathbf{q}}^{\mathbf{T}}\mathbf{M}\dot{\mathbf{q}}}{2} - \frac{\mathbf{q}^{\mathrm{T}}\mathbf{K}\mathbf{q}}{2}, \tag{3.12}$$

where

$$\mathbf{M} = \mathrm{diag}(0_1, \ldots, 0_M, M_1, \ldots, M_N) \tag{3.13}$$

and

$$\mathbf{K} = \mathrm{diag}(0_1, \ldots, 0_M, K_1, \ldots, K_N). \tag{3.14}$$

The virtual work carried out by the excitation force applied on the shell is

$$\delta W = \mathbf{Q}^{\mathbf{T}}\delta\mathbf{q}, \tag{3.15}$$

where $\mathbf{Q}$ is the generalized force vector

$$\mathbf{Q}(t) = F\sin(\Omega t)\begin{bmatrix} 0_1 & \cdots & 0_M & W_1(0,0) & \cdots & W_N(0,0) \end{bmatrix}^{\mathbf{T}}. \tag{3.16}$$

(d) Nonlinear coupled equation

From equations (3.7) and (3.12), it follows that the Lagrangian function for the shell–fluid-coupled system

$$L(\boldsymbol{\varphi}, \mathbf{q}) = \left(-\frac{\boldsymbol{\varphi}^{\mathbf{T}} \mathbf{C} \boldsymbol{\varphi}}{2} - \dot{\boldsymbol{\varphi}}^{\mathbf{T}} \mathbf{b} - V_{\mathrm{F}} \right) + \frac{\dot{\mathbf{q}}^{\mathbf{T}} \mathbf{M} \dot{\mathbf{q}} - \mathbf{q}^{\mathbf{T}} \mathbf{K} \mathbf{q}}{2}. \tag{3.17}$$

The variational stationary conditions of the functional (2.3) with respect to its variable vectors $\boldsymbol{\varphi}$ and $\mathbf{q}$ give the following coupled equations

$$\mathbf{C}\boldsymbol{\varphi} - \mathbf{B}\dot{\mathbf{q}} = \mathbf{0}, \tag{3.18}$$

and

$$\mathbf{M}\ddot{\mathbf{q}} + \mathbf{K}\mathbf{q} + \partial \frac{\left[\boldsymbol{\varphi}^{\mathbf{T}} \mathbf{C}(\mathbf{q}) \boldsymbol{\varphi}\right]}{(2\partial \mathbf{q})} + \frac{\partial V_{\mathrm{F}}}{\partial \mathbf{q}} + \mathbf{B}^{\mathbf{T}} \dot{\boldsymbol{\varphi}} = \mathbf{Q}, \tag{3.19}$$

where the elements of matrix $\mathbf{B}$ are given by

$$B_{ij} = \frac{\partial b_i}{\partial q_j}, \quad i = 1 \quad 2 \quad \cdots \quad L \quad j = 1 \quad 2 \quad \cdots \quad M + N. \tag{3.20}$$

As shown in expression (3.8), the matrix $\mathbf{C}$ involves the kinetic energy of the fluid and it is definitely positive, so that from equation (3.18) it follows that

$$\boldsymbol{\varphi} = \mathbf{C}^{-\mathbf{1}} \mathbf{B} \dot{\mathbf{q}}, \tag{3.21}$$

and

$$\dot{\boldsymbol{\varphi}} = \mathbf{C}^{-\mathbf{1}} \mathbf{B} \ddot{\mathbf{q}} + \dot{\mathbf{q}}^{\mathrm{T}} \left[\frac{\partial (\mathbf{C}^{-\mathbf{1}} \mathbf{B})}{\partial \mathbf{q}} \right] \dot{\mathbf{q}}. \tag{3.22}$$

Substituting (3.21) and (3.22) into (3.19), we obtain

$$\mathbf{M}\ddot{\mathbf{q}} + \mathbf{K}\mathbf{q} + \frac{1}{2} (\dot{\mathbf{q}}^{\mathbf{T}} \mathbf{B}^{\mathbf{T}} \mathbf{C}^{-1}) \left(\frac{\partial \mathbf{C}}{\partial \mathbf{q}} \right) (\mathbf{C}^{-\mathbf{1}} \mathbf{B} \dot{\mathbf{q}}) + \frac{\partial V_{\mathrm{F}}}{\partial \mathbf{q}} + \mathbf{B}^{\mathbf{T}} (\mathbf{C}^{-\mathbf{1}} \mathbf{B} \ddot{\mathbf{q}}) + \mathbf{B}^{\mathbf{T}} \left(\dot{\mathbf{q}}^{T} \frac{\partial (\mathbf{C}^{-\mathbf{1}} \mathbf{B})}{\partial \mathbf{q}} \dot{\mathbf{q}} \right) = \mathbf{Q}, \tag{3.23}$$

which can be further transformed into the form

$$\frac{\mathrm{d}(\mathbf{m}\dot{\mathbf{q}})}{\mathrm{d}t} + \mathbf{M}\ddot{\mathbf{q}} + \mathbf{K}\mathbf{q} + \frac{\partial V_{\mathrm{F}}}{\partial \mathbf{q}} - \frac{\partial (\dot{\mathbf{q}}^{\mathbf{T}} \mathbf{m} \dot{\mathbf{q}}/2)}{\partial \mathbf{q}} = \mathbf{Q}, \tag{3.24}$$

where

$$\mathbf{m} = \mathbf{B}^{\mathbf{T}} \mathbf{C}^{-\mathbf{1}} \mathbf{B}. \tag{3.25}$$

In this coupled equation, the solid matrices $\mathbf{M}$ and $\mathbf{K}$ are constant symmetric matrices, whereas the fluid matrix $\mathbf{m}$ and the fluid gravity potential function V_{F} given in appendix B are functions of $\mathbf{q}$.

(e) Coupled fluid–structure interaction equation in the mode form

To reveal nonlinear interactions of FSI vibration modes, as presented in appendix B, equation (3.24) is linearized by expanding matrix $\mathbf{m}$ and potential V_{F} to Taylor series of $\mathbf{q}$.

Therefore, we have

$$\mathbf{m} = \mathbf{m}^{(0)} + q_k \mathbf{m}_k^{(1)} + \cdots, \tag{3.26}$$

and

$$V_{\mathrm{F}} = V^{(0)} + q_i V_i^{(1)} + \frac{k_{ij}^{(0)} q_i q_j}{2} + \frac{k_{rij}^{(1)} q_r q_i q_j}{6} + \cdots, \tag{3.27}$$

where $\mathbf{m}^{(0)}, \mathbf{m}_k^{(1)}, \mathbf{k}^{(0)}, \mathbf{k}_r^{(1)}$ are symmetric matrices with constant elements. Substituting (3.26) and (3.27) into (3.24) yields

$$\begin{aligned}&\mathbf{m}^{(0)}\ddot{\mathbf{q}} + \dot{q}_k \mathbf{m}_k^{(1)}\dot{\mathbf{q}} + q_k \mathbf{m}_k^{(1)}\ddot{\mathbf{q}} + \mathbf{M}\ddot{\mathbf{q}} + \mathbf{K}\mathbf{q} + \mathbf{V}^{(1)} + \mathbf{k}^{(0)}\mathbf{q} + q_k \mathbf{k}_k^{(1)}\mathbf{q} \\ &\quad + \tfrac{1}{2}\left[\mathbf{q}^{\mathrm{T}}\mathbf{k}_1^{(1)}\mathbf{q} \quad \cdots \quad \mathbf{q}^{\mathrm{T}}\mathbf{k}_{M+N}^{(1)}\mathbf{q}\right]^T - \tfrac{1}{2}\left[\dot{\mathbf{q}}^{\mathrm{T}}\mathbf{m}_1^{(1)}\dot{\mathbf{q}} \quad \cdots \quad \dot{\mathbf{q}}^{\mathrm{T}}\mathbf{m}_{M+N}^{(1)}\dot{\mathbf{q}}\right]^T + \cdots = \mathbf{Q},\end{aligned} \tag{3.28}$$

which is further linearized as

$$\tilde{\mathbf{m}}^{(0)}\ddot{\mathbf{q}} + \tilde{\mathbf{k}}\mathbf{q} = \mathbf{Q} - \mathbf{V}^{(1)}, \quad \tilde{\mathbf{m}} = \mathbf{m}^{(0)} + \mathbf{M} \quad \text{and} \quad \tilde{\mathbf{k}} = \mathbf{k}^{(0)} + \mathbf{K}, \tag{3.29}$$

where $\mathbf{V}^{(1)}$ represents a constant generalized force vector caused by the gravitational force of the fluid. Because only dynamic response is of interest, this constant force vector is ignored in the following analysis. The natural modes and the corresponding eigenvalues (the squares of natural frequencies) are obtained as

$$\boldsymbol{\Psi} = \begin{bmatrix}\boldsymbol{\psi}_1 & \boldsymbol{\psi}_2 & \cdots & \boldsymbol{\psi}_{M+N}\end{bmatrix} \quad \text{and} \quad \boldsymbol{\Lambda} = \mathrm{diag}(\omega_1^2, \omega_2^2, \ldots, \omega_{M+n}^2), \tag{3.30}$$

satisfying the orthogonal relationships

$$\boldsymbol{\Psi}^{\mathrm{T}}\tilde{\mathbf{m}}\boldsymbol{\Psi} = \mathbf{I} \quad \text{and} \quad \boldsymbol{\Psi}^{\mathrm{T}}\tilde{\mathbf{k}}\boldsymbol{\Psi} = \boldsymbol{\Lambda}. \tag{3.31}$$

Using the mode transformation

$$\mathbf{q} = \boldsymbol{\Psi}\mathbf{x} \quad \text{and} \quad \mathbf{x} = \begin{bmatrix}x_1 & x_2 & \cdots & x_{M+N}\end{bmatrix}^{\mathrm{T}}, \tag{3.32}$$

and retaining the first order of nonlinearity, we transform equation (3.28) into the mode form

$$\begin{aligned}&(\mathbf{I} + q_k(\mathbf{x})\bar{\mathbf{m}}_k)\ddot{\mathbf{x}} + (\boldsymbol{\Lambda} + q_k(\mathbf{x})\bar{\mathbf{k}}_k)\mathbf{x} + \dot{q}_k(\mathbf{x})\bar{\mathbf{m}}_k\dot{\mathbf{x}} + \tfrac{1}{2}\boldsymbol{\Psi}^{\mathbf{T}}\left[\mathbf{x}^{\mathbf{T}}\bar{\mathbf{k}}_1\mathbf{x} \quad \cdots \quad \mathbf{x}^{\mathbf{T}}\bar{\mathbf{k}}_{M+N}\mathbf{x}\right]^{\mathrm{T}} \\ &\quad - \tfrac{1}{2}\boldsymbol{\Psi}^{\mathbf{T}}\left[\dot{\mathbf{x}}^{\mathbf{T}}\bar{\mathbf{m}}_1\dot{\mathbf{x}} \quad \cdots \quad \dot{\mathbf{x}}^{\mathbf{T}}\bar{\mathbf{m}}_{M+N}\dot{\mathbf{x}}\right]^{\mathrm{T}} = \boldsymbol{\Psi}^{\mathrm{T}}\mathbf{Q},\end{aligned} \tag{3.33}$$

where

$$\bar{\mathbf{m}}_k = \boldsymbol{\Psi}^{\mathrm{T}}\mathbf{m}_k^{(1)}\boldsymbol{\Psi}, \quad \bar{\mathbf{k}}_k = \boldsymbol{\Psi}^{\mathbf{T}}\mathbf{k}_k^{(1)}\boldsymbol{\Psi}, \quad q_k(\mathbf{x}) = \boldsymbol{\Psi}^{(k)}\mathbf{x}. \tag{3.34}$$

Here, $\boldsymbol{\Psi}^{(k)}$ represent the kth line vector of the matrix $\boldsymbol{\Psi}$. Left multiplying equation (3.33) by $(\mathbf{I} + \sum_{\mathbf{k}} q_k(x)\mathbf{m}_{\mathbf{k}})^{-1}$ and omitting higher nonlinear items than second-order yields

$$\begin{aligned}&\ddot{\mathbf{x}} + (\mathbf{I} - q_k(\mathbf{x})\bar{\mathbf{m}}_k)\boldsymbol{\Lambda}\mathbf{x} + q_k(\mathbf{x})\bar{\mathbf{k}}_k\mathbf{x} + \dot{q}_k(\mathbf{x})\bar{\mathbf{m}}_k\dot{\mathbf{x}} + \tfrac{1}{2}\boldsymbol{\Psi}^{\mathbf{T}}\left[\mathbf{x}^{\mathbf{T}}\bar{\mathbf{k}}_1\mathbf{x} \quad \cdots \quad \mathbf{x}^{\mathbf{T}}\bar{\mathbf{k}}_{M+N}\mathbf{x}\right]^{\mathrm{T}} \\ &\quad - \tfrac{1}{2}\boldsymbol{\Psi}^{\mathbf{T}}\left[\dot{\mathbf{x}}^{\mathbf{T}}\bar{\mathbf{m}}_1\dot{\mathbf{x}} \quad \cdots \quad \dot{\mathbf{x}}^{\mathbf{T}}\bar{\mathbf{m}}_{M+N}\dot{\mathbf{x}}\right]^{\mathrm{T}} = (\mathbf{I} - q_k(\mathbf{x})\bar{\mathbf{m}}_k)\boldsymbol{\Psi}^{\mathrm{T}}\mathbf{Q}.\end{aligned} \tag{3.35}$$

Equation (3.35) includes the square nonlinearity items on the left-hand side and the parametric excitation items on the right-hand side [16]. Equation (3.35) establishes a basis for the following numerical investigations.

4. An experimental case analysis

In this section, we will apply the theoretical model and method developed earlier to investigate an example of an experiment to validate the proposed theory.

(a) Experimental case

Here, we investigate an experimental example with the geometrical parameters: $a = 0.103\,\mathrm{m}$, $H = 0.213\,\mathrm{m}$, $\Delta h = 0.0045\,\mathrm{m}$, $d = 0.135\,\mathrm{m}$. The material properties of the glass shell are mass density $\rho_S = 2.777 \times 10^3\,\mathrm{kg\,m^{-3}}$, elastic module $E = 9.65 \times 10^{10}\,\mathrm{N\,m^{-2}}$ and Poisson's ratio $\nu = 0.25$. The mass density of the water is $\rho_F = 1.0 \times 10^3\,\mathrm{kg\,m^{-3}}$. The shell is horizontally excited by an electromagnetic exciter powered by an amplifier that amplifies a sinusoidal signal from a signal generator to produce the excitation force. A force sensor is arranged between the exciter and shell surface to measure and to monitor the force frequency and amplitude, which are controlled by adjusting the signal level from the generator and amplifier. The excitation frequency range is about 181.6 Hz near to the first higher natural frequency, measured by the experiment, with the mode $\cos 2\theta$ of the coupling system (figure 2*a*). Three gravity waves were observed in the experiments as shown in figure 2. Figure 2*b* shows the first axisymmetric wave of natural frequency 3.02 Hz aroused by an excitation of frequency 184 Hz and magnitude 3.6 N, from which the Ritz function $J_0(\lambda_{0,1}r)$ is chosen. The second wave shown in figure 2*c* is aroused by an excitation of 185 Hz and 5.4 N, which has the natural frequency 3.57 Hz and wavenumber 4 corresponding to a water surface function $J_4(\lambda_{4,1}r)\cos 4\theta$. The third one shown in figure 2*d* is aroused by an excitation of 186 Hz and 7.8 N, which behaves as the second axisymmetric wave of frequency 4.11 Hz suggesting a water surface function $J_0(\lambda_{0,2}r)$.

The experiments demonstrated that (i) the appearances of different gravity waves depended on the amplitudes and frequencies of the excitation force; (ii) with time developing, there existed a transition phenomenon between different gravity waves for a given frequency and amplitude of the excitation force. These experimental observation results will be examined using our theoretical analysis as follows.

(b) Theoretical equations with four-mode approximations

To investigate and to explore the nonlinear phenomenon observed in this experiment, based on the Ritz functions listed in appendix A, we set up a four-mode interaction model by equations (3.4)–(3.6) with $L = 16$, $M = 8$ and $N = 4$. Using the method discussed in §3, we derive nonlinear equation (3.35) into the following form:

$$\left.\begin{aligned}
\ddot{x}_1 &= -2\mu_1\omega_1\dot{x}_1 - \omega_1^2 x_1 + F(8.12x_2 - 9.32x_3 - 10.7x_4)\cos\Omega t \\
&\quad + (-1.29\times 10^7 x_1x_2 + 1.46\times 10^7 x_1x_3 + 1.68\times 10^7 x_1x_4) \\
&\quad + (9.40\dot{x}_1\dot{x}_2 - 10.7\dot{x}_1\dot{x}_3 - 12.3\dot{x}_1\dot{x}_4) + 0.874F\cos\Omega t, \\
\ddot{x}_2 &= -2\mu_2\omega_2\dot{x}_2 - \omega_2^2 x_2 - 10.4x_1F\cos\Omega t \\
&\quad + (1.62\times 10^7 x_1^2 + 6.84\times 10^3 x_2^2 + 3.19\times 10^3 x_2x_3 + 2.71\times 10^4 x_3^2 - 1.35\times 10^4 x_4^2) \\
&\quad + (-16.6\dot{x}_1^2 - 8.60\dot{x}_2^2 - 79.1\dot{x}_2\dot{x}_3 - 35.2\dot{x}_3^2 + 20.9\dot{x}_4^2), \\
\ddot{x}_3 &= -2\mu_3\omega_3\dot{x}_3 - \omega_3^2 x_3 + 3.45x_1F\cos\Omega t \\
&\quad + (-5.39\times 10^6 x_1^2 + 1.47\times 10^3 x_2^2 + 2.00\times 10^4 x_2x_3 + 1.74\times 10^4 x_3^2 + 4.92\times 10^3 x_4^2) \\
&\quad + (9.27\dot{x}_1^2 + 35.5\dot{x}_2^2 - 8.06\dot{x}_2\dot{x}_3 - 12.6\dot{x}_3^2 + 2.66\dot{x}_4^2) \\
\text{and}\quad \ddot{x}_4 &= -2\mu_4\omega_4\dot{x}_4 - \omega_4^2 x_4 + 6.72x_1F\cos\Omega t \\
&\quad + (-1.05\times 10^7 x_1^2 - 1.51\times 10^3 x_2x_4 + 1.92\times 10^4 x_3x_4) \\
&\quad + (13.8\dot{x}_1^2 + 10.6\dot{x}_2\dot{x}_4 - 24.4\dot{x}_3\dot{x}_4).
\end{aligned}\right\} \tag{4.1}$$

Here, x_1 corresponds to the first higher natural mode in the form $\cos 2\theta$, and x_2, x_3, x_4 involve the gravity waves associated with $J_0(\lambda_{0,1}r)$, $J_0(\lambda_{0,2}r)$, $J_4(\lambda_{4,1}r)\cos 4\theta$, respectively. The corresponding

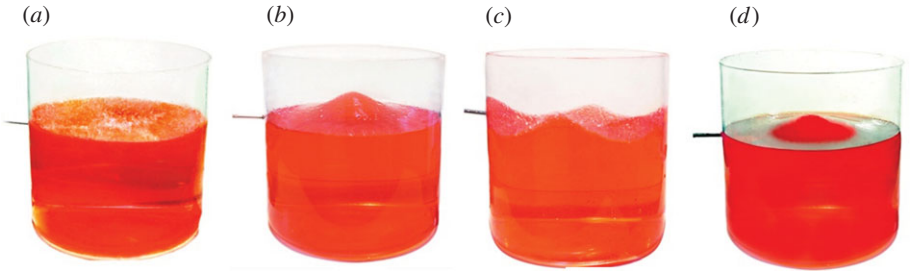

Figure 2. Photos of the linear and nonlinear surface waves at excitation frequency near to 181.6 Hz: (*a*) linear response; (*b*) gravity wave $J_0(\lambda_{0,1}r)$, (*c*) gravity wave $J_4(\lambda_{4,1}r)\cos 4\theta$ and (*d*) gravity wave $J_0(\lambda_{0,2}r)$. (Online version in colour.)

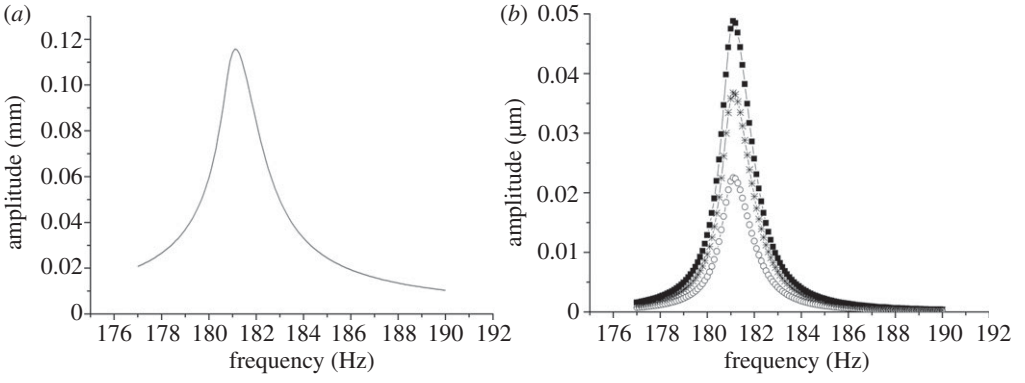

Figure 3. The frequency–response curves ($F = 1.5$ N): (*a*) for mode coordinates x_1 (solid line), and (*b*) for mode coordinates x_2 (filled square), x_3 (circle), and x_4 (asterisks).

frequencies are

$$\omega_1 = 2\pi \cdot 181.6, \quad \omega_2 = 2\pi \cdot 3.02, \quad \omega_3 = 2\pi \cdot 4.11 \quad \text{and} \quad \omega_4 = 2\pi \cdot 3.57.$$

To consider the practical damping effect, we respectively introduced the following four-mode damping coefficients into equations (4.1)

$$\mu_1 = 0.00435, \quad \mu_2 = 0.0065, \quad \mu_3 = 0.008 \quad \text{and} \quad \mu_4 = 0.0068.$$

Because there is no available theory and method to estimate/calculate the damping of the coupled system from known fluid/solid viscosities, these non-dimensional damping coefficients have to be measured by the corresponding experiments using the decaying rate method based on the recorded time histories of the responses.

(c) Force amplitudes and frequencies for exciting gravity waves

To explore the effect of amplitudes and frequencies of the excitation force on the appearance of gravity waves in this nonlinear FSI system, we fix a force amplitude then sweep its frequency from 176 to 190 Hz to solve equation (4.1) using a fifth-order Runge–Kutta–Fehlberg algorithm [17]. From these numerical calculations, we can find the suitable amplitude and frequency to excite a gravity wave.

Figure 3 shows the amplitude response curves of mode coordinates x_1, x_2, x_3 and x_4 when the excitation force amplitude is 1.5 N. Because the amplitude of the force is small, these response curves behave as the shapes for linearized system.

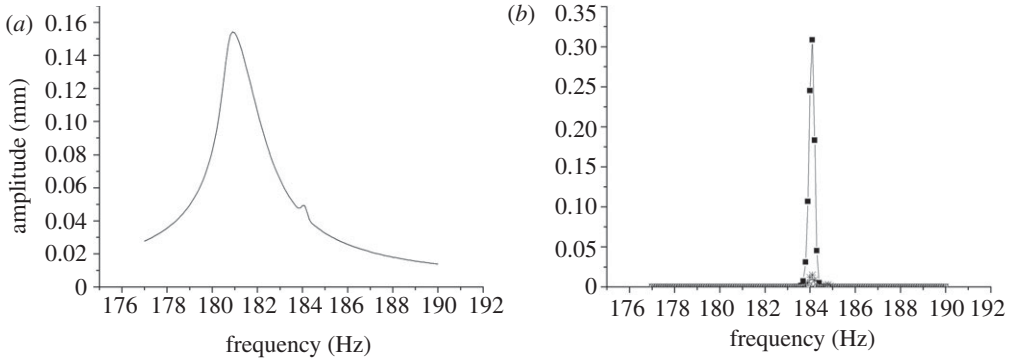

Figure 4. The frequency–response curves ($F = 2$ N): (*a*) for mode coordinates x_1 (solid line), and (*b*) for mode coordinates x_2 (filled square), x_3 (circle), and x_4 (asterisks).

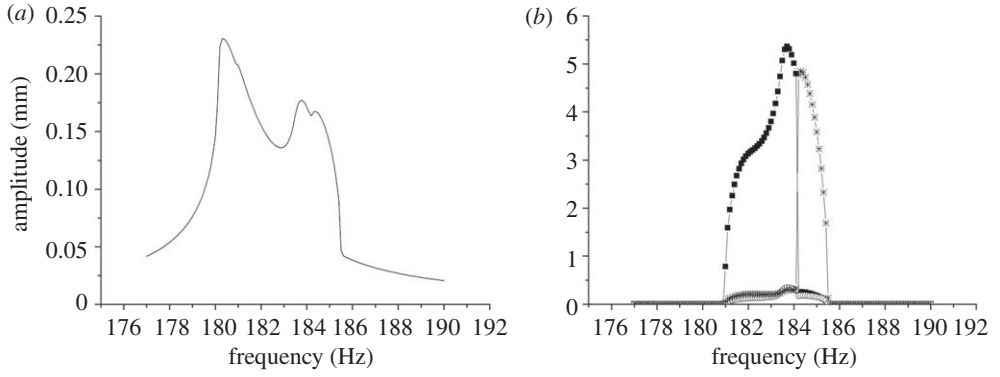

Figure 5. The frequency–response curves ($F = 3$ N): (*a*) for mode coordinates x_1 (solid line), and (*b*) for mode coordinates x_2 (filled square), x_3 (circle), and x_4 (asterisks).

Figure 4 presents the frequency–response curves for the excitation force amplitude 2 N. In this excitation, as shown by figure 4*a*, an extra peak at about 184 Hz, when compared with figure 3*a*, is observed. At this frequency, the amplitude of x_2 is impetuously increased, as indicated by figure 4*b*, which implies the appearance of gravity wave $J_0(\lambda_{0,1}r)$.

With the excitation force amplitude increased to 3 N, the frequency–response curves show the shapes given in figure 5. There are two peaks (figure 5*a*) which appeared at about 183.7 and 184.4 Hz, respectively. The amplitudes of x_2 and x_4 are impetuously increased at about these two frequencies, which imply that the gravity waves $J_0(\lambda_{0,1}r)$ and $J_4(\lambda_{4,1}r)\cos 4\theta$ are excited. The calculation demonstrates that the gravity wave $J_0(\lambda_{0,1}r)$ appears in an excitation frequency range of 181–184 Hz, whereas the gravity wave $J_4(\lambda_{4,1}r)\cos 4\theta$ appears in an excitation frequency range of 184–186 Hz.

Figure 6 presents the frequency–response curves when the excitation force is 4.5 N, which shows that all three gravity waves are aroused. The gravity wave $J_0(\lambda_{0,1}r)$ appears in the excitation frequency range of 179.3–183.6 Hz, whereas the gravity waves $J_4(\lambda_{4,1}r)\cos 4\theta$ and $J_0(\lambda_{0,2}r)$ appear in the excitation frequency range of 183.7–185.7 and 185.7–186.2 Hz, respectively.

Furthermore, sweeping the excitation frequency from 175 to 188 Hz, and varying the amplitude of excitation force from 0 to 11 N, we obtained the critical force–frequency curves as shown in figure 7. F_{01}, F_{02} and F_{41} denote the critical forces associated with the gravity waves $J_0(\lambda_{0,1}r)$, $J_1(\lambda_{0,2}r)$ and $J_4(\lambda_{4,1}r)\cos 4\theta$, respectively. When the force amplitude and frequency is above these curves, the corresponding gravity waves would be aroused, while below these curves

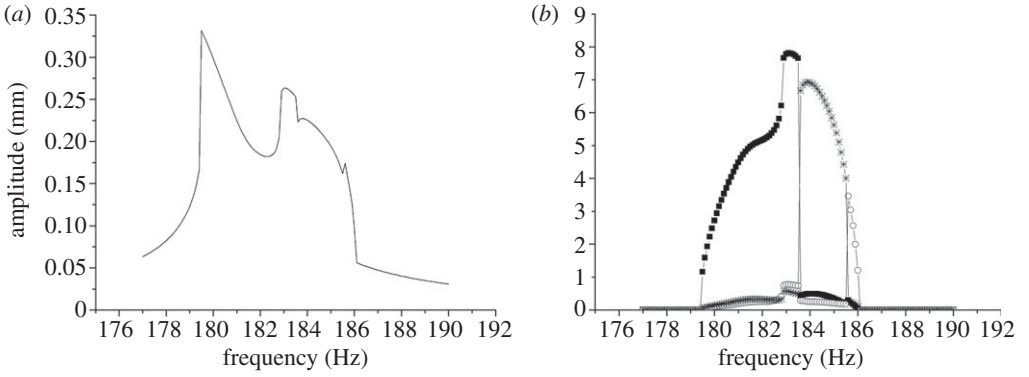

Figure 6. The frequency–response curves ($F = 4.5$ N): (*a*) for mode coordinates x_1 (solid line), and (*b*) for mode coordinates x_2 (filled square), x_3 (circle), and x_4 (asterisks).

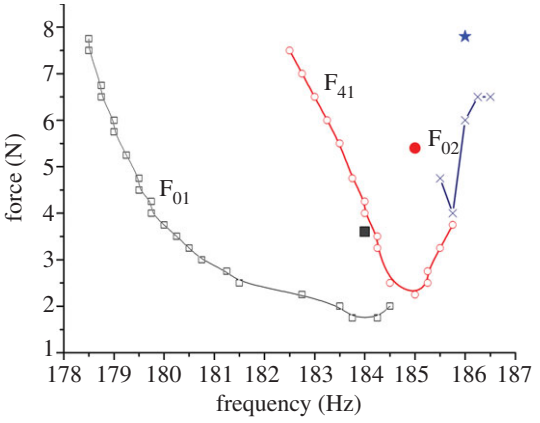

Figure 7. Critical force–frequency curves for gravity waves $J_0(\lambda_{0,1}r)$, $J_4(\lambda_{4,1}r)\cos 4\theta$ and $J_0(\lambda_{0,2}r)$. Open square, F_{01}; open circle, F_{41}; cross, F_{02}. (Online version in colour.)

there would be no gravity waves aroused. The black solid square, red dot and blue star represent the experimental observation points described in §4*a*. Figure 7 shows that experimental points are located exactly within regions predicted by the theoretical model.

It is worth mentioning that from figure 7 sufficient large amplitudes of excitation force with frequency equal to or below the high natural frequency 181.6 Hz of x_1 may excite gravity waves. This finding agrees with experimental observations of Shen [10]. However, previous researches by Huntley [4] and Mahony & Smith [5] concluded that no gravity wave occurred for this frequency region.

(d) Response spectrum analysis

Following the results obtained in §4*c*, we have learnt the suitable amplitude and frequency for exciting a gravity wave of the nonlinear system. For a linear system, the dynamic response frequency is the same as the frequency of the excitation force. What is the frequency spectrum of the dynamic response of this nonlinear system excited by a chosen amplitude and frequency of excitation force? To address this problem, we calculate the dynamic responses of the system excited by a force of amplitude (4.5 N) and frequency (183 Hz), in which the gravity wave $J_0(\lambda_{0,1}r)$ is expected to be excited. Figure 8 presents the spectrum of x_1 and x_2. The spectrum of x_1

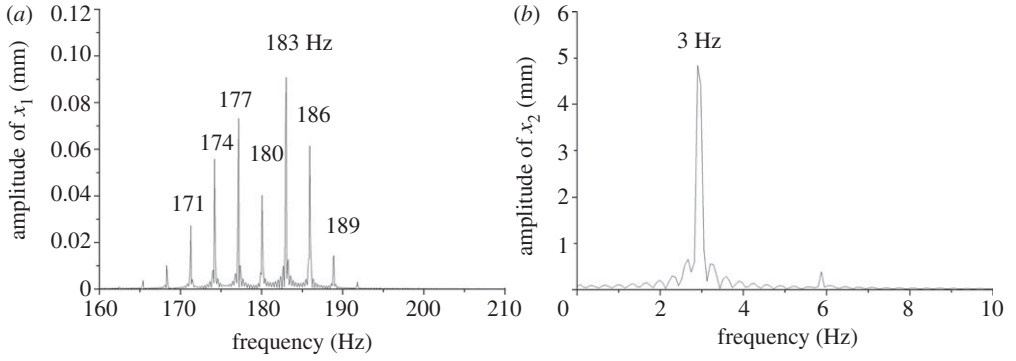

Figure 8. Spectrum of x_1 and x_2, when $F = 4.5$ N, excitation frequency = 183 Hz.

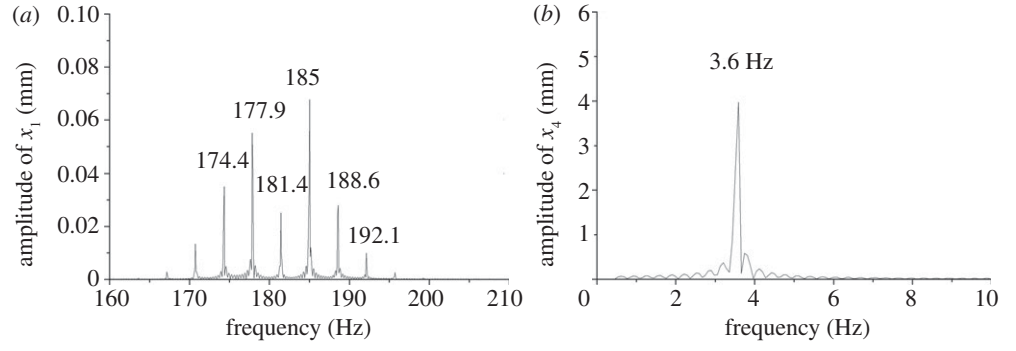

Figure 9. Spectrum of x_1 and x_4, when $F = 4.5$ N, excitation frequency = 185 Hz.

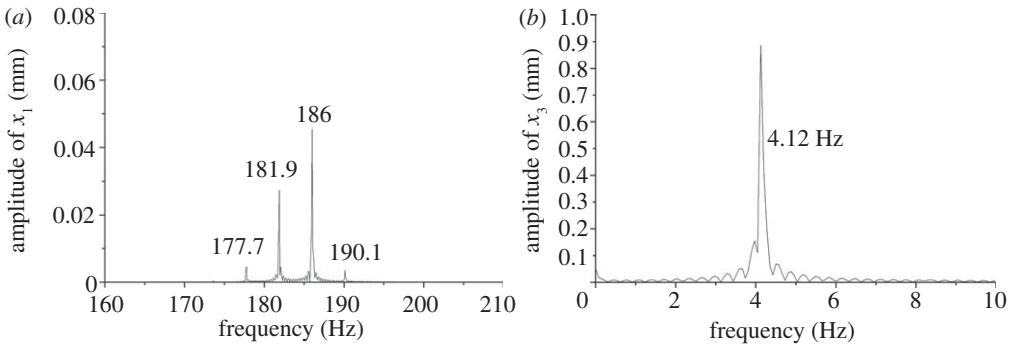

Figure 10. Spectrum of x_1 and x_3, when $F = 4.5$ N, excitation frequency = 186 Hz.

includes about 11 frequency components of which the main energy lies in the frequency range of 171–189 Hz, whereas the spectrum of x_2 shows the dominant frequency 3 Hz of the gravity wave $J_0(\lambda_{0,1}r)$. For this nonlinear system, a high-frequency excitation force excites a lower frequency gravity wave.

Figures 9 and 10 provide another two spectra with different force amplitudes and frequencies when gravity wave $J_0(\lambda_{0,1}r)$ or $J_4(\lambda_{4,1}r)\cos 4\theta$ is aroused. These spectra agree with experimental observations by Li [9] and Shen [10].

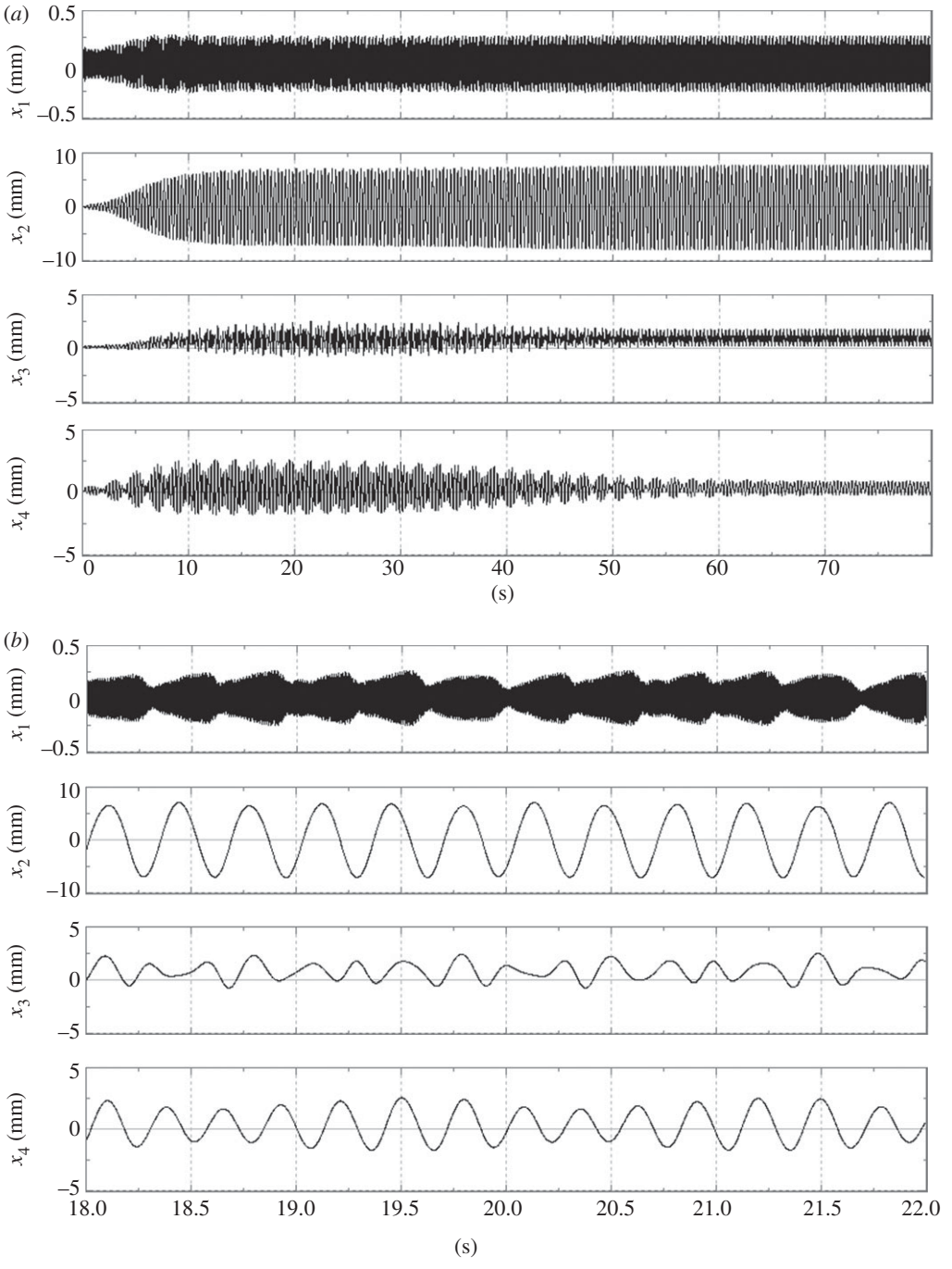

Figure 11. The time histories of x_1–x_4 of the system excited by a force of amplitude 5.71 N and frequency 183.5 Hz: (*a*) 0–80, and (*b*) 18–22 s.

(e) Transitions between different gravity waves

In the experiments by Shen [10], it was observed that for certain excitation frequencies and force amplitudes, there was a transition between different gravity waves. A typical phenomenon shows that the amplitude of gravity wave $J_4(\lambda_{4,1}r)\cos 4\theta$ initially was large but then reduced to very

small after several seconds, and at the same time the amplitude of gravity wave $J_0(\lambda_{0,1}r)\cos 0\theta$ tended to a large stable value.

To explain this phenomenon, the time histories for x_1–x_4 from equation (4.1) are numerically calculated. Figure 11 shows these time histories obtained for the force of frequency 183.5 Hz and amplitude 5.71 N with the static initial conditions. These time histories obviously indicate that at about 20 s the amplitudes of variables x_2, x_3 and x_4 reach their maximum values, respectively. However, with the time increasing, the amplitudes of x_3 (wave mode $J_0(\lambda_{0,2}r)$) and x_4 (wave mode $J_4(\lambda_{4,1}r)\cos 4\theta$) tend their smaller stationary values, respectively, whereas the amplitude of x_2 (wave mode $J_0(\lambda_{0,1}r)\cos 0\theta$) reaches a large stationary value. These results agree with the experimentally observed phenomenon by Shen [10].

5. Conclusion and discussion

We have addressed the nonlinear phenomenon of low-frequency gravity water waves aroused by high-frequency excitation on a cylindrical shell partially filled with water by investigating nonlinear water–shell dynamic interactions. Based on a variational principle, the governing equations and numerical equations describing nonlinear FSI dynamics of a shell–water system are derived. The nonlinear interaction equations in mode form are constructed by retaining the first-order nonlinear items in derivations.

A four-mode interaction model is constructed which is used to analyse an experiment system. Numerical calculations are carried out to predict the excitation force–frequency regions exciting three gravity wave modes. The obtained time histories and spectrum analysis demonstrate the experimentally observed phenomena including the gravity wave modes transition.

Comparing with previous studies concentrating only on the water waves in the fluid domain excited by prescribed vessel motions, the theoretical model presented in this paper considers nonlinear FSI; therefore, new findings amend the previous researches:

— Mahony & Smith [5] developed an acoustic air–water wave interaction model which, theoretically, could not be directly applied to the glass shell–water system by Huntley [6]. Our study considers the elastic shell–water system, based on which the nonlinear responses of the shell-modulated vibration mode are theoretically predicted other than a single harmonic linear response was assumed by Huntley [6];
— by deductions from the basic Hamiltonian of the coupled system, the motion of shell and fluid is explicitly described as function of external excitation, other than the conjectural components assumed by Mahony & Smith [5]. The developed model therefore gives quantitative prediction of the critical force–frequency curve other than simple qualitative predictions;
— this study demonstrated that parametric nonlinearity exists in the system, which extends the instability region to excitation frequencies equal or below the natural frequency with sufficient large excitation amplitudes, as verified by experimental observations. However, previous researches by Huntley [4] and Mahony & Smith [5] predicted that excitation force should be infinite when excitation frequency is equal to or below the natural frequency; and
— this paper successfully predicted the transition between different gravity waves, which agrees with experimental observations.

For further researches, it is worth clarifying the following three issues. First, we tested a model, including surface tension effects, and a very small difference result was obtained when compared with the model with no surface tension consideration. Therefore, to simplify the model, we omitted the surface tension in this paper. In this coupled problem, for mode shape on the free surface of the high-frequency resonance, both linear theory and experiments reveal that the capillary wave component is relatively very small compared with the gravity wave components, surface tension is therefore not critical, so that the potential from surface tension is neglected.

For other problems, if surface tension effects are important, the surface tension can be included to get more accurate results. Furthermore, we did not consider water splashing cases, which is supported by our experimental observations: when carefully tuning the excitation force to a certain magnitude, the investigated phenomenon occurs without splashing. Therefore, based on our experiments with suitable excitation forces, we do not consider the slashing breaking waves, which is an important challenge research topic investigated by Terwagne & Bush [18] while studying Tibetan singing bowls. The last one involves half-frequency resonances, which may have a significant influence on the whole system, although it is not considered in this paper. A possible investigation on this type of resonance for fluid–water interaction systems may be considered.

The authors acknowledge the National Science Foundation of China for supporting this research under grant nos 10572101 and 19872003.

Appendix A

The functions of kinetic and potential energies of the shell and the Rayleigh–Ritz functions used in the paper.

The functions used in this paper are listed in table 1.

Appendix B

Parameter expansions of the nonlinear functions.

The movable integral region for the functions is shown in figure 12.

1. The gravity potential of the dynamic fluid

$$\begin{aligned}
V_{\mathrm{F}} &= \rho_{\mathrm{F}} \int\int\int gz \,\mathrm{d}v = \rho_{\mathrm{F}} g \left[\int_0^{2\pi} \int_0^{a} \int_{-d}^{0} zr \,\mathrm{d}z \,\mathrm{d}r \,\mathrm{d}\theta + \int_0^{2\pi} \int_0^{a} \int_0^{\eta} zr \,\mathrm{d}z \,\mathrm{d}r \,\mathrm{d}\theta \right. \\
&\quad \left. + \int_0^{2\pi} \int_{-d}^{0} \int_a^{a+w} zr \,\mathrm{d}r \,\mathrm{d}z \,\mathrm{d}\theta + \int_0^{2\pi} \int_a^{a+w} \int_0^{\eta} zr \,\mathrm{d}z \,\mathrm{d}r \,\mathrm{d}\theta \right] + \cdots \\
&= \frac{1}{2}\rho_{\mathrm{F}} g \left(\int_0^{2\pi} \int_0^{a} \eta^2 r \,\mathrm{d}r \,\mathrm{d}\theta - \pi a^2 \,\mathrm{d}^2 \right) + \rho_{\mathrm{F}} g \int_0^{2\pi} \int_{-d}^{0} z \left(aw + \frac{1}{2} w^2 \right) \mathrm{d}z \,\mathrm{d}\theta \\
&\quad + \frac{1}{2}\rho_{\mathrm{F}} g \int_0^{2\pi} \int_a^{a+w} \eta^2 r \,\mathrm{d}r \,\mathrm{d}\theta + \cdots \\
&= \frac{1}{2}\rho_{\mathrm{F}} g \left(\sum_{i=1}^{N} \sum_{j=1}^{N} \eta_i \eta_j \int_0^{2\pi} \int_0^{a} H_i H_j r \,\mathrm{d}r \,\mathrm{d}\theta - \pi a^2 d^2 \right) \\
&\quad + \rho_{\mathrm{F}} g \sum_{k=1}^{L} \left(w_k \int_0^{2\pi} \int_{-d}^{0} z W_k a \,\mathrm{d}z \,\mathrm{d}\theta + \frac{1}{2} \sum_{s=1}^{L} w_k w_s \int_0^{2\pi} \int_{-d}^{0} z W_k W_s \,\mathrm{d}z \,\mathrm{d}\theta \right) \\
&\quad + \frac{1}{2}\rho_{\mathrm{F}} g \sum_{i=1}^{N} \sum_{j=1}^{N} \sum_{k=1}^{L} \eta_i \eta_j w_k \int_0^{2\pi} (H_i H_j W_k)_{\substack{z=0 \\ r=a}} a \,\mathrm{d}\theta + \cdots . \qquad \text{(B 1)}
\end{aligned}$$

Rewrite (B 1) into a matrix form

$$V_{\mathrm{F}} = V^{(0)} + q_i V_i^{(1)} + \frac{1}{2} k_{ij}^{(0)} q_i q_j + \frac{1}{6} k_{kij}^{(1)} q_k q_i q_j + \cdots , \qquad \text{(B 2)}$$

where

$$V^{(0)} = \frac{1}{2}\rho_{\mathrm{F}} g \pi a^2 \,\mathrm{d}^2 \qquad \text{(B 3)}$$

Table 1. The functions of kinetic and potential energies of the shell and the Rayleigh–Ritz functions.

function	formulation
T_s	$\frac{1}{2}\rho_s \Delta h \int_0^{2\pi}\int_{-d}^{H-d} (\dot{u}^2+\dot{v}^2+\dot{w}^2) a \,\mathrm{d}z\,\mathrm{d}\theta$
V_s	$\frac{E\Delta h}{2(1-\nu^2)}\int_0^{2\pi}\int_{-d}^{H-d}\left\{\left(\left[\frac{\partial u}{\partial z}+\frac{1}{a}\left(\frac{\partial v}{\partial \theta}+w\right)\right]^2-\frac{2(1-\nu)}{a}\left[\frac{\partial u}{\partial z}\left(\frac{\partial v}{\partial \theta}+w\right)\right]\right.\right.$ $\left.+\frac{(1-\nu)}{2}\left[\frac{1}{a}\frac{\partial u}{\partial \theta}+\frac{\partial v}{\partial z}\right]^2\right)+\frac{\Delta h^2}{12}\left(\left[\frac{\partial^2 w}{\partial z^2}+\frac{1}{a^2}\left(\frac{\partial^2 w}{\partial \theta^2}-\frac{\partial v}{\partial \theta}\right)\right]^2$ $-\frac{2(1-\nu)}{a^2}\left[\frac{\partial^2 w}{\partial z^2}\left(\frac{\partial^2 w}{\partial \theta^2}-\frac{\partial v}{\partial \theta}\right)\right]+\frac{2(1-\nu)}{a^2}\left[\frac{\partial^2 w}{\partial z\partial \theta}-\frac{\partial v}{\partial z}\right]^2\Bigg)\Bigg\} a\,\mathrm{d}z\,\mathrm{d}\theta$
$W_1(\theta,z)$	$46.447\,(z+d)-643.426(z+d)^2+3217(z+d)^3-6563(z+d)^4$
$W_2(\theta,z)$	$10.666\,(z+d)\cos 2\theta$
$W_3(\theta,z)$	$[40.64\,(z+d)-540.44(z+d)^2+2303.96(z+d)^3-3826.05(z+d)^4]\cos 2\theta$
$W_4(\theta,z)$	$11.638\,(z+d)\cos 4\theta$
$H_1(r,\theta)$	$J_0(\lambda_{0,1}r)$
$H_2(r,\theta)$	$J_0(\lambda_{0,2}r)$
$H_3(r,\theta)$	$J_2(\lambda_{2,1}r)\cos 2\theta$
$H_4(r,\theta)$	$J_2(\lambda_{2,2}r)\cos 2\theta$
$H_5(r,\theta)$	$J_2(\lambda_{2,3}r)\cos 2\theta$
$H_6(r,\theta)$	$J_2(\lambda_{2,84}r)\cos 2\theta$
$H_7(r,\theta)$	$J_2(\lambda_{2,85}r)\cos 2\theta$
$H_8(r,\theta)$	$J_4(\lambda_{4,1}r)\cos 4\theta$
$\Phi_1(r,\theta,z)$	$J_0(\lambda_{0,1}r)\cosh[\lambda_{0,1}(z+d)]/\cosh(\lambda_{0,1}d)$
$\Phi_2(r,\theta,z)$	$J_0(\lambda_{0,2}r)\cosh[\lambda_{0,2}(z+d)]/\cosh(\lambda_{0,2}d)$
$\Phi_3(r,\theta,z)$	$J_2(\lambda_{2,1}r)\cos 2\theta\cosh[\lambda_{2,1}(z+d)]/\cosh(\lambda_{2,1}d)$
$\Phi_4(r,\theta,z)$	$J_2(\lambda_{2,2}r)\cos 2\theta\cosh[\lambda_{2,2}(z+d)]/\cosh(\lambda_{2,2}d)$
$\Phi_5(r,\theta,z)$	$J_2(\lambda_{2,3}r)\cos 2\theta\cosh[\lambda_{2,3}(z+d)]/\cosh(\lambda_{2,3}d)$
$\Phi_6(r,\theta,z)$	$J_2(\lambda_{2,84}r)\cos 2\theta\cosh[\lambda_{2,84}(z+d)]/\cosh(\lambda_{2,84}d)$
$\Phi_7(r,\theta,z)$	$J_2(\lambda_{2,85}r)\cos 2\theta\cosh[\lambda_{2,85}(z+d)]/\cosh(\lambda_{2,85}d)$
$\Phi_8(r,\theta,z)$	$J_4(\lambda_{4,1}r)\cos 4\theta\cosh[\lambda_{4,1}(z+d)]/\cosh(\lambda_{4,1}d)$
$\Phi_9(r,\theta,z)$	$I_0(\pi r/d)/(\sqrt{2}I_0(\pi a/d))$
$\Phi_{10}(r,\theta,z)$	$\cos 2\theta\cdot r^2/(\sqrt{2}a^2)$
$\Phi_{11}(r,\theta,z)$	$\cos(\pi z/d)\cos 2\theta I_2(\pi r/d)/I_2(\pi a/d)$
$\Phi_{12}(r,\theta,z)$	$\cos(2\pi z/d)\cos 2\theta I_2(2\pi r/d)/I_2(2\pi a/d)$
$\Phi_{13}(r,\theta,z)$	$\cos(3\pi z/d)\cos 2\theta I_2(3\pi r/d)/I_2(3\pi a/d)$
$\Phi_{14}(r,\theta,z)$	$\cos(4\pi z/d)\cos 2\theta I_2(4\pi r/d)/I_2(4\pi a/d)$
$\Phi_{15}(r,\theta,z)$	$\cos 4\theta\cdot r^4/(\sqrt{2}a^4)$
$\Phi_{16}(r,\theta,z)$	$\cos(\pi z/d)\cos 4\theta I_4(\pi r/d)/I_4(\pi a/d)$

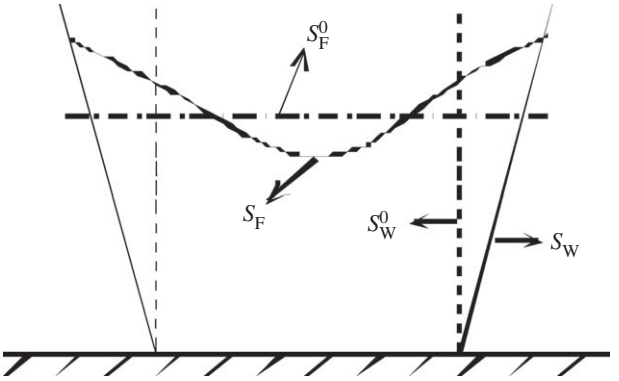

Figure 12. The moveable integral region.

and

$$\mathbf{V}^{(1)} = \rho_F g \left[0 \cdots 0_M \int_0^{2\pi} \int_{-d}^{0} zW_1 a \, dz \, d\theta \cdots \int_0^{2\pi} \int_{-d}^{0} zW_N a \, dz \, d\theta \right]^T, \tag{B 4}$$

as well as $k_{ij}^{(0)}$ and $k_{ij}^{(1)}$ represent the element (line i and column j) of the matrices $\mathbf{k}^{(0)}$ and $\mathbf{k}_k^{(1)}$ (or $\mathbf{k}_l^{(1)}$), respectively. Using the subindex range: $i = 1, 2, \ldots, M$; $j = 1, 2, \ldots, N$; $k = 1, \ldots, M$ and $l = M+1, \ldots, M+N$, we write these matrices in equation (B 2) in the following matrix forms:

$$\mathbf{k}^{(0)} = \begin{bmatrix} \mathbf{k}_{\mathbf{I}}^{(0)} & \mathbf{0} \\ \mathbf{0} & \mathbf{k}_{\mathbf{II}}^{(0)} \end{bmatrix}, \tag{B 5}$$

$$\mathbf{k}_k^{(1)} = \begin{bmatrix} \mathbf{0} & \mathbf{k}_{\mathbf{I}k}^{(1)} \\ \mathbf{k}_{\mathbf{I}k}^{(1)\mathrm{T}} & \mathbf{0} \end{bmatrix} \tag{B 6}$$

and

$$\mathbf{k}_l^{(1)} = \begin{bmatrix} \mathbf{k}_{\mathbf{II}l}^{(1)} & \mathbf{0} \\ \mathbf{0} & \mathbf{0} \end{bmatrix}, \tag{B 7}$$

$$\mathbf{k}_{\mathbf{I}ij}^{(0)} = \rho_F g \int_0^{2\pi} \int_0^{a} H_i H_j r \, dr \, d\theta, \tag{B 8}$$

$$\mathbf{k}_{\mathbf{II}ij}^{(0)} = \rho_F g \int_0^{2\pi} \int_{-d}^{0} zW_i W_j \, dz \, d\theta, \tag{B 9}$$

$$\mathbf{k}_{\mathbf{I}kij}^{(1)} = \rho_F g \int_0^{2\pi} (H_k H_i W_j)_{\substack{z=0 \\ r=a}} a \, d\theta \tag{B 10}$$

and

$$\mathbf{k}_{\mathbf{II}lij}^{(1)} = \rho_F g \int_0^{2\pi} (H_i H_j W_{l-M})_{\substack{z=0 \\ r=a}} a \, d\theta. \tag{B 11}$$

2. The gravity mass matrix $\mathbf{M}_F$ of the fluid

The matrix $\mathbf{M}_F$ depends on the vector $\mathbf{b}$ and matrix $\mathbf{C}$. The element of vector $\mathbf{b}$ is given by

$$\begin{aligned} b_i &= \rho_F \iiint_{\Omega} \Phi_i \, dv \\ &= \rho_F \left[\int_0^{2\pi} \int_0^{a} \int_{-d}^{0} \Phi_i r \, dz \, dr \, d\theta + \int_0^{2\pi} \int_0^{a} \int_0^{\eta} \Phi_i r \, dz \, dr \, d\theta \right. \\ &\quad \left. + \int_0^{2\pi} \int_{-d}^{0} \int_a^{a+w} \Phi_i r \, dr \, dz \, d\theta + \int_0^{2\pi} \int_a^{a+w} \int_0^{\eta} \Phi_i r \, dz \, dr \, d\theta \right] + \cdots \end{aligned}$$

$$= \rho_F \int_0^{2\pi}\int_0^a\int_{-d}^0 \Phi_i r\,\mathrm{d}z\,\mathrm{d}r\,\mathrm{d}\theta + \rho_F \int_0^{2\pi}\int_0^a \left(\Phi_i|_{z=0}\,\eta + \frac{1}{2}\left.\frac{\partial \Phi_i}{\partial z}\right|_{z=0}\eta^2\right) r\,\mathrm{d}r\,\mathrm{d}\theta$$
$$+ \rho_F \int_0^{2\pi}\int_0^a \left[\Phi_i|_{r=a}\,w + \frac{1}{2}\left(\Phi_i + \frac{1}{a}\frac{\partial \Phi_i}{\partial r}\right)\Big|_{r=a} w^2\right] a\,\mathrm{d}z\,\mathrm{d}\theta + \rho_F \int_0^{2\pi} (\Phi_i \eta w)\,{}_{z=0}^{r=a}\, a\,\mathrm{d}\theta + \cdots$$
$$= \rho_F \left(\int_0^{2\pi}\int_0^a\int_{-d}^0 \Phi_i r\,\mathrm{d}z\,\mathrm{d}r\,\mathrm{d}\theta + \sum_{i=1}^m \eta_j \int_0^{2\pi}\int_0^a \Phi_i|_{z=0}\,H_j r\,\mathrm{d}r\,\mathrm{d}\theta\right.$$
$$\left. + \frac{1}{2}\sum_{j=1}^m\sum_{i=1}^m \eta_j\eta_l \int_o^{2\pi}\int_0^a \left.\frac{\partial \Phi_i}{\partial z}\right|_{z=0} H_j H_l r\,\mathrm{d}r\,\mathrm{d}\theta\right)$$
$$+ \rho_F \left(\sum_{k=1}^n w_k \int_0^{2\pi}\int_{-d}^0 \Phi_i|_{r=a}\,W_k a\,\mathrm{d}z\,\mathrm{d}\theta\right.$$
$$\left. + \frac{1}{2}\sum_{k=1}^n\sum_{s=1}^n w_k w_s \int_0^{2\pi}\int_{-d}^0 \left(\Phi_i + \frac{1}{a}\frac{\partial \Phi_i}{\partial r}\right)_{r=a} W_k W_s a\,\mathrm{d}z\,\mathrm{d}\theta\right)$$
$$+ \rho_F \sum_{j=1}^m\sum_{k=1}^n \eta_j w_k \int_0^{2\pi} (\Phi_i H_j W_k)\,{}_{r=a}^{z=0}\, a\,\mathrm{d}\theta + \cdots. \tag{B 12}$$

The matrix $\mathbf{B}$ is defined by

$$\mathbf{B} = \frac{\partial \mathbf{b}}{\partial \mathbf{q}} = \mathbf{B}^{(0)} + \sum_{k=1}^{M+N} q_k \mathbf{B}_k^{(1)} + \cdots, \tag{B 13}$$

where

$$\mathbf{B}^{(0)} = \left[\mathbf{B}_{\mathbf{I}^{(0)}} \quad \mathbf{B}_{\mathbf{II}}^{(0)}\right] \text{ and } \mathbf{B}_k^{(1)} = \left[\mathbf{B}_{\mathbf{I}k}^{(1)} \quad \mathbf{B}_{\mathbf{II}k}^{(1)}\right], \tag{B 14}$$

in which

$$B_{\mathbf{I}ij}^{(0)} = \rho_F \int_0^{2\pi}\int_0^a \Phi_i|_{z=0}\,H_j r\,\mathrm{d}r\,\mathrm{d}\theta \tag{B 15}$$
$$B_{\mathbf{II}in}^{(0)} = \rho_F \int_0^{2\pi}\int_{-d}^0 \Phi_i|_{r=a}\,W_n a\,\mathrm{d}z\,\mathrm{d}\theta, \tag{B 16}$$
$$B_{\mathbf{I}kij}^{(1)} = \rho_F \int_0^{2\pi}\int_0^a \left(\frac{\partial \Phi_i}{\partial z}\right)_{z=0} H_j H_k r\,\mathrm{d}r\,\mathrm{d}\theta \tag{B 17}$$
$$B_{\mathbf{II}kij}^{(1)} = \rho_F \int_0^{2\pi} (\Phi_i W_j H_k)\,{}_{r=a}^{z=0}\, a\,\mathrm{d}\theta \tag{B 18}$$
$$\mathbf{B}_{\mathbf{I}lij}^{(1)} = \rho_F \int_0^{2\pi} (\Phi_i W_{l-M} H_j)\,{}_{r=a}^{z=0}\, a\,\mathrm{d}\theta \tag{B 19}$$
and
$$\mathbf{B}_{\mathbf{II}lij}^{(1)} = \rho_F \int_0^{2\pi}\int_{-d}^0 \left(\Phi_i + \frac{1}{a}\frac{\partial \Phi_i}{\partial r}\right)_{r=a} W_{l-M} W_j a\,\mathrm{d}z\,\mathrm{d}\theta\Big|, \tag{B 20}$$

and the subindices ranges are: $i = 1, 2, \ldots, L$; $n = 1, 2, \ldots, N$; $j = 1, 2, \ldots, M$; $k = 1, 2, \ldots, M$; $l = (M+1), \ldots, (M+N)$.

3. The matrix $\mathbf{C}$

$$\begin{aligned} C_{ij} &= \rho_{\mathrm{F}} \iiint_{\Omega} \nabla\Phi_i \cdot \nabla\Phi_j \,\mathrm{d}v \\ &= \rho_{\mathrm{F}} \int_{-d}^{0}\int_{0}^{2\pi}\int_{0}^{a} (\nabla\Phi_i \cdot \nabla\Phi_j) r \,\mathrm{d}r\,\mathrm{d}\theta\,\mathrm{d}z \\ &\quad + \sum_{k=1}^{M} \eta_k \rho_{\mathrm{F}} \int_{0}^{2\pi}\int_{0}^{a} (\nabla\Phi_i \cdot \nabla\Phi_j)_{z=0} H_k r \,\mathrm{d}r\,\mathrm{d}\theta \\ &\quad + \sum_{s=1}^{N} w_s \rho_{\mathrm{F}} \int_{0}^{2\pi}\int_{-d}^{0} (\nabla\Phi_i \cdot \nabla\Phi_j)_{r=a} W_s a \,\mathrm{d}z\,\mathrm{d}\theta + \cdots, \end{aligned} \tag{B 21}$$

which is expanded as

$$\mathbf{C} = \mathbf{C}^{(0)} + \sum_{k=1}^{M+N} q_k \mathbf{C}_k^{(1)} + \cdots, \tag{B 22}$$

where

$$C_{ij}^{(0)} = \rho_{\mathrm{F}} \int_{-d}^{0}\int_{0}^{2\pi}\int_{0}^{a} (\nabla\Phi_i \cdot \nabla\Phi_j) r \,\mathrm{d}r\,\mathrm{d}\theta\,\mathrm{d}z, \tag{B 23}$$

$$C_{kij}^{(1)} = \begin{cases} \rho_{\mathrm{F}} \displaystyle\int_{0}^{2\pi}\int_{0}^{a} (\nabla\Phi_i \cdot \nabla\Phi_j)_{z=0} H_k r \,\mathrm{d}r\,\mathrm{d}\theta, & k \le M \\ \rho_{\mathrm{F}} \displaystyle\int_{0}^{2\pi}\int_{-d}^{0} (\nabla\Phi_i \cdot \nabla\Phi_j)_{r=a} W_{k-M} a \,\mathrm{d}z\,\mathrm{d}\theta, & M < k \le M+N \end{cases} \tag{B 24}$$

4. The matrix $\mathbf{m}$

From equation (3.33), it follows that

$$\mathbf{m} = \mathbf{B}^{\mathbf{T}} \mathbf{C}^{-\mathbf{1}} \mathbf{B}. \tag{B 25}$$

Substituting (B 13) and (B 22) into (B 24), we obtain

$$\begin{aligned} \mathbf{m} &= \left(\mathbf{B}^{(0)} + \sum_{k=1}^{M+N} q_k \mathbf{B}_k^{(1)}\right)^{\mathbf{T}} \left(\mathbf{C}^{(0)} + \sum_{k=1}^{M+N} q_k \mathbf{C}_k^{(1)}\right)^{-\mathbf{1}} \left(\mathbf{B}^{(0)} + \sum_{k=1}^{M+N} q_k \mathbf{B}_k^{(1)}\right) + \cdots \\ &= \mathbf{B}^{(0)\mathrm{T}} \mathbf{C}^{(0)-1} \mathbf{B}^{(0)} \\ &\quad + \sum_{k=1}^{M+N} q_k (\mathbf{B}_k^{(1)\mathrm{T}} \mathbf{C}^{(1)-\mathbf{1}} \mathbf{B}^{(0)} + \mathbf{B}^{(0)} \mathbf{C}^{(0)-1} \mathbf{B}_k^{(1)} - \mathbf{B}^{(0)\mathrm{T}} \mathbf{C}^{(0)-\mathbf{1}} \mathbf{C}\mathbf{I}_{\mathbf{k}} \mathbf{C}^{(0)-\mathbf{1}} \mathbf{B}^{(0)}) + \cdots, \end{aligned} \tag{B 26}$$

Let

$$\mathbf{m} \equiv \mathbf{m}^{(0)} + \sum_{k=1}^{M+N} q_k \mathbf{m}_k^{(1)} + \cdots, \tag{B 27}$$

then

$$\mathbf{m}^{(0)} = \mathbf{B}^{(0)\mathbf{T}} \mathbf{C}^{(0)-\mathbf{1}} \mathbf{B}^{(0)} \tag{B 28}$$

and

$$\mathbf{m}_k^{(1)} = \mathbf{B}_k^{(1)\mathbf{T}} \mathbf{C}^{(0)-\mathbf{1}} \mathbf{B}^{(0)} + \mathbf{B}^{(0)} \mathbf{C}^{(0)-\mathbf{1}} \mathbf{B}_k^{(1)} - \mathbf{B}^{(0)\mathbf{T}} \mathbf{C}^{(0)-\mathbf{1}} \mathbf{C}_k^{(1)} \mathbf{C}^{(0)-\mathbf{1}} \mathbf{B}^{(0)}. \tag{B 29}$$

References

1. Benjamin TB, Ursell F. 1954 The stability of the plane free surface of a liquid in vertical periodic motion. *Proc. R. Soc. Lond. A* **225**, 505–515. (doi:10.1098/rspa.1954.0218)

2. Couder Y, Protière S, Fort E, Boudaoud A. 2005 Dynamical phenomena: walking and orbiting droplets. *Nature* **437**, 208. (doi:10.1038/437208a)
3. Guckenheimer J, Holmes P. 1983 *Nonlinear oscillations, dynamical systems, and bifurcations of vector fields*. New York, NY: Springer.
4. Huntley I. 1972 Observations on a spatial-resonance phenomenon. *J. Fluid Mech.* **53**, 209–216. (doi:10.1017/S0022112072000114)
5. Mahony JJ, Smith R. 1972 On a model representation for certain spatial-resonance phenomena. *J. Fluid Mech.* **53**, 193–207. (doi:10.1017/S0022112072000102)
6. Huntley I. 1977 Spatial resonance of a liquid-filled vibrating beaker. *J. Fluid Mech.* **80**, 81–97. (doi:10.1017/S0022112077001542)
7. Wei QD, Wang, DJ, Yan B, Du XD, Chen J. 1997 A visualization study on water spray of dragon washbasin. In *Atlas of visualization*, ch. 11, pp. 169–179. Boca Raton, FL: CRC Press. (The visualization society of Japan)
8. Hsieh DY, Denissenko P. 1998 Water waves in a circular elastic vessel: the experiment. In *American Physical Society/Division of Fluid Dynamics 51st Annual Meeting*, 22–24 November, 1998, Philadelphia, PA.
9. Li J. 2000 Experimental study on mechanical phenomenon of the Chinese cultural relic: dragon washbasin. Postdoctoral research report (in Chinese). Peking University, Beijing.
10. Shen S. 2003 Study on nonlinear vibrations of liquid–solid coupled system of an elastic liquid storage shell. Postdoctoral research report (in Chinese). Peking University, Beijing.
11. Hsieh DY. 2000 Theory of water waves in an elastic vessel. *Acta Mech. Sin.* **16**, 97–112. (doi:10.1007/BF02486701)
12. Luke JC. 1967 A variational principle for a fluid with a free surface. *J. Fluid Mech.* **27**, 395–397. (doi:10.1017/S0022112067000412)
13. Seliger RL, Whitham GB. 1968 Variational principles in continuum mechanics. *Proc. R. Soc. Lond. A* **305**, 1–25. (doi:10.1098/rspa.1968.0103)
14. Xing JT, Price WG. 1997 Variational principles of nonlinear dynamical fluid–solid interaction systems. *Phil. Trans. R. Soc. Lond. A* **355**, 1063–1095. (doi:10.1098/rsta.1997.0053)
15. MacDonald JK. 1933 Successive approximations by the Rayleigh–Ritz variation method. *Phys. Rev.* **43** 830–833. (doi:10.1103/PhysRev.43.830)
16. Nayfeh AH, Mook DT. 1979 *Nonlinear oscillations*. New York, NY: Wiley.
17. Hairer E, Nørsett SP, Wanner G. 1993 *Solving ordinary differential equations I: nonstiff problems*. Berlin, Germany: Springer.
18. Terwagne D, Bush JWM. 2011 Tibetan singing bowls. *Nonlinearity* **24**, R51–R66. (doi:10.1088/0951-7715/24/8/R01)